Uncertainties in the Finite Time Lyapunov Exponent in an ocean ensemble prediction model

Mateusz Matuszak[1], Johannes Röhrs[1], Pål Erik Isachsen[1 2], and Martina Idžanović[1]

[1]Norwegian Meteorological Institute, Henrik Mohns Plass 1, 0371 Oslo, Norway

[2]Department of Geosciences, University of Oslo, P.O. Box 1022, Blindern, 0315 Oslo, Norway

Correspondence: Mateusz Matuszak (mateuszm@met.no)

Abstract. Lagrangian coherent structures (LCS) are transient features in ocean circulation that describe particle transport, revealing information about transport barriers and accumulation or dispersion regions. Finite time Lyapunov exponents (FTLE) approximate LCSs under certain conditions, and are here used to characterize flow field features and their uncertainties in predictions from a regional ocean forecast system. Generally, Lagrangian trajectories as well as FTLE analysis inherit uncertainty from the underlying ocean model, bearing substantial uncertainties as a result of chaotic and turbulent flow fields. In addition, velocity fields and resulting FTLE evolve rapidly. We investigate the uncertainty of FTLE fields at any given time using an ensemble prediction system (EPS) to propagate velocity field uncertainty into the FTLE analysis. Variability in time and ensemble realisations is evaluated. Averaging over ensemble members can reveal robust FTLE ridges, i.e. FTLE ridges that exist across ensemble realisations. Time averages reveal persistent FTLE ridges, i.e. FTLE ridges that occur over extended periods of time. We find that FTLE features are generally more robust than persistent for the chosen time interval. Large scale FTLE ridges are more robust and persistent than small scale FTLE ridges. Averaging of FTLE field is effective at removing chaotic, short-lived and unpredictable structures and may provide the means to employ FTLE analysis in forecasting applications that require to separate uncertain from certain flow features.

1 Introduction

Ocean currents transport and disperse various environmental tracers, such as nutrients, plankton and pollution. Studying and predicting such transport is of interest and importance for environmental management, especially in the coastal zone. Prediction typically relies on the use of Oceanic General Circulation Models (OGCMs), in which the nonlinear governing equations of motion are first integrated numerically to determine a velocity field, and where this field is then used to calculate transport and spreading of (synthetic) tracers or particles. In many applications, the aim is not necessarily an exact tracking of individual particles as much as the identification of regions of high or low particle concentration as well as flow features that may act as dynamical barriers between such regions. To this end, the concept of Lagrangian Coherent Structures (LCS) has received increased attention from the oceanographic community. As the name suggests, LCSs are coherently evolving features in unsteady and chaotic flow fields that can systematically influence particle trajectories (Haller and Yuan, 2000; Tang et al., 2010; Farazmand and Haller, 2012; Haller, 2015). More specifically, LCSs describe coherent morphological features of the flow

field that cause accumulation, spreading and deformation, and they can even suggest the presence of transport barriers. LCSs have therefore found applications in both process studies and emergency responses, e.g. man-over-board scenarios and oil-spill clean-ups (e.g. Haller and Yuan, 2000; Lekien et al., 2005; Olascoaga and Haller, 2012; Peacock and Haller, 2013; Dong et al., 2021).

Various methods have been proposed to find LCSs in observed or modeled velocity fields (e.g. d'Ovidio et al., 2004; Shadden et al., 2005; Haller, 2011; Duran et al., 2018). Among those, the Finite-Time Lyapunov Exponent (FTLE) presents an approximation of LCS that is objective and straightforward to apply (Hadjighasem et al., 2017), and is capable of highlighting areas of particle accumulation or spreading—depending on whether it is computed forward or backward in time—for the spatial and temporal scales on which coastal ocean surface flow varies (e.g. Giudici et al., 2021; Ghosh et al., 2021; Lou et al., 2022). More specifically, the FTLE describes the stretching that a fluid parcel at a given location experiences over a finite time due to the spatially and temporally-varying velocity field. Elongated patches of elevated FTLE values—hereafter referred to as FTLE ridges—may be interpreted as boundaries between coherent structures (flow features identifiable due to their longevity compared to other nearby flows), that is, boundaries between flow features such as eddies, vortices or meandering jets; and it is near such boundaries that a fluid parcel's motion will change drastically (Hussain, 1983; Samelson, 2013; Balasuriya et al., 2016). In unstable flows, FTLE ridges define time-varying regions exhibiting either an attraction to or repulsion from hyperbolic trajectories (Shadden et al., 2005; Lee et al., 2007; Brunton and Rowley, 2010; Balasuriya, 2012; Balasuriya et al., 2016; van Sebille et al., 2018; Krishna et al., 2023). Under certain conditions, these FTLE ridges may reveal LCSs (Farazmand and Haller, 2012) and provide a diagnostic tool for describing fluid flows that is pertinent to applications of particle transport.

Using FTLE analysis as a detection for LCS has limitations. For example, a sheared current is not an LCS but will result in high FTLE values, or the detected FTLE ridge may be far away from a true LCS (see example 3 and 4 in Haller (2011)). While more complete methods LCS detection exist (e.g. Duran et al., 2018), this article will focus on FTLE analysis since it provides a straightforward gridded spatial description of Lagrangian transport characteristics that can be analyzed using elementary statistical methods. Given its ease of implementation, we ultimately aim to examine the potential use of FTLE analysis as a practical tool for applications in operational oceanography, e.g. oil-spill modeling.

More specifically, the current study will examine the usefulness of an FTLE approach to transport and dispersion modeling in light of the *uncertain* nature of any ocean model forecast. Due to the nonlinear and highly chaotic nature of real ocean flows—as well as the flow in high-resolution ocean models—small errors in the knowledge or specification of the velocity field may yield large perturbations in estimated particle trajectories. Furthermore, even with a perfect knowledge of the velocity field, uncertainties in particle's initial position or time of release may grow into large uncertainties over time. Thus, despite the potential usefulness of LCS or FTLE analysis outlined above, the need to address the uncertainty and errors in e.g. the underlying current velocity remains. Can the uncertainty in forecasted FTLE fields be quantified? A common way to address prediction uncertainties in geophysical flow fields is by use of Ensemble Prediction Systems (EPS). Instead of issuing one single deterministic integration of the circulation model, an ensemble of model realisations is obtained by time-integrating the model with variations in the initial conditions and boundary conditions (e.g. the atmospheric forcing). The ensemble is hence

intended to span out the possible states of the system (e.g. Lebreton et al., 2012; Idžanović et al., 2023). While common in weather prediction, this method is in its infancy in regional ocean prediction (Thoppil et al., 2021).

The impact of general flow variability on FTLE and other LCS analyses has received some attention, specifically related to the question of whether time-persistent features can be identified in a nonlinear and chaotic flow field (e.g. Olascoaga et al., 2006; Gouveia et al., 2020; Dong et al., 2021). There has also been some studies aiming to address uncertainty aspect, using ocean EPSs. (e.g. Wei et al., 2013; Guo et al., 2016; Wei et al., 2016; Balasuriya, 2020; Zimmermann et al., 2024). Here, we wish to further elaborate on how FTLE analysis can give information on coherent flow structures, despite the presence of time variability and uncertainty in the forecast. We specifically distinguish between *persistence* and *robustness* of flow features: We refer to persistence in relation to flow features that remain at their location over an extended period of time, hence provide usefulness for applications that use an analysis and assume the flow field remains in a similar state. Then we refer to robustness in a prediction of flow features if a majority of a model's ensemble members indicate a similar outcome such that the forecasted FTLE have a high probability to be realized in nature.

Our study region will be the continental shelf, continental slope and deep ocean basin off Lofoten-Veseterålen in Northern Norway, a region of considerable importance for both the marine climate and marine ecosystem in the northern North-Atlantic. In section 2, we describe the operational EPS ocean forecast system for this region and provide an outline of how the FTLE analysis is performed. In section 3 we present results invoking time-averages and ensemble averages of FTLE fields, respectively. In section 4, we draw conclusions on temporal and seasonal variability of FTLE and uncertainties in the FTLE analysis. Finally, we discuss implications on the applicability of the FTLE analysis in uncertain flow fields as a tool in operational forecasting.

2   Data and methods

2.1   Study region

The bathymetry and modelled surface currents around Lofoten-Vesterålen (LoVe) archipelago along northern Norway's coast are shown in Figure 1. The continental shelf sea off LoVe is know to be a hot spot for fisheries due to its high concentrations of nutrients, which form feeding grounds and spawning banks for marine life (Sundby and Bratland, 1987; Sundby et al., 2013). Transport of relevant nutrients has been widely studied (e.g. Adlandsvik and Sundby, 1994; Röhrs et al., 2014), and the Finite-Size Lyapunov Exponent (FSLE) analysis presented in Dong et al. (2021) shed light on possible mechanisms for cross-slope transport of nutrients that could play a role in sustaining biological production.

The LoVe region is characterized by complex bottom topography and a steep continental slope that steer the region's primary large-scale currents (Sundby, 1984), namely the Norwegian Atlantic Slope Current (NwASC) (Rossby et al., 2009) and the Norwegian Coastal Current (NCC) (Gascard et al., 2004). The complex coastline and the Vestfjorden embayment directly guide the path of the NCC, and also cause complex flow features, including strong tidal currents through through Moskstraumen—one of the many straits that cut through the archipelago (Børve et al., 2021). During winter, southerly winds enhance the onshore

Ekman transport and water mass accumulation along the coast, thus speeding up the large-scale currents after geostrophic adjustment (Mitchelson-Jacob and Sundby, 2001).
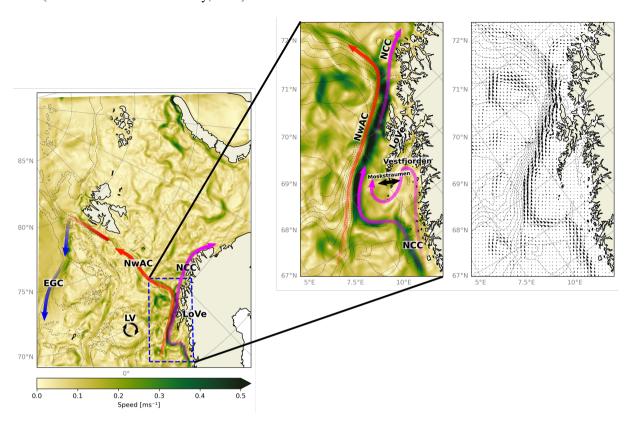

Figure 1. Average ocean current speed $[ms^{-1}]$ for the period 2023-02-01 to 2023-02-28 over the full Barents-2.5 model domain. Dashed blue lines highlight the region of interest for this study, which is the oceanic part around the Lofoten-Vesterålen islands (LoVe) and is enlarged. Arrows in the rightmost panel indicate average current velocities for the period. Bathymetry is indicated by gray dashed lines. Purple arrows indicate the Norwegian Coastal Current (NCC). Red arrows indicate the Norwegian Atlantic Current (NwAC). Blue arrows indicate the East Greenland Current (EGC). The circular black arrows indicate the Lofoten Vortex (LV). The two-headed black arrow indicates Moskstraumen.

The NwASC and NCC meet right off the LoVe archipelalgo. The steep continental slope, combined with a narrow shelf, sets up steep fronts that host a range of flow instabilities. The result is the most intense mesoscale eddy field in all of the Nordic Seas and vigorous exchanges of heat, salt and nutrients between the shelf and deep ocean. (Koszalka et al., 2013; Isachsen, 2015; Trodahl and Isachsen, 2018). As such, the region offers a particular challenge with respect to accurate modeling of currents and transport.

2.2 Regional Ocean Ensemble Prediction System

We use flow data from Barents-2.5 EPS (Röhrs et al., 2023), an ensemble prediction system based on the Regional Ocean Modeling System (ROMS; Shchepetkin and McWilliams, 2005). The model has a 2.5 km horizontal grid size and hourly

temporal resolution, covering the Barents Sea, the coast off northern Norway and Svalbard (see Fig. 1). The EPS consists of 24 members, divided into four sets of six members. The sets are initiated with a 6-hour delay, at 00 UTC, 06 UTC, 12 UTC, and 18 UTC, with a forecast period of 66 hours. Each member is initialized by its own state from the previous day in order to preserve sufficient spread in the ensemble. The EPS forecast is initialized with perturbed initial conditions in the mesoscale

105   circulation to represent model uncertainties. The ensemble spread is further controlled by the Ensemble Kalman Filter data assimilation scheme, which controls the spread of observed variables (Evensen, 1994; Röhrs et al., 2023). The first member in each set (four members) is forced by the most recent atmospheric conditions from the AROME-Arctic model (Müller et al., 2017). The remaining members are forced by 20 members drawn from the integrated forecast system developed by the European Centre for Medium Range Weather Forecasts (ECWF-ENS) (Röhrs et al., 2023).
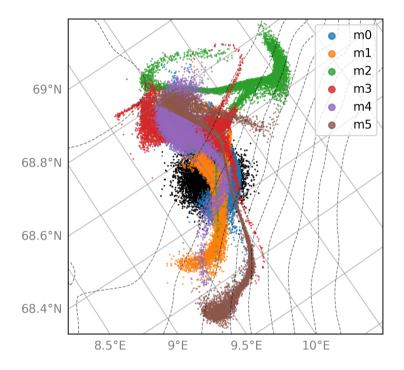

Figure 2. A particle cluster advected for 48 hours from 2023-02-01 using velocity fields from six Barents-2.5 EPS members. Black dots mark the particle clusters initial position.

110   A detailed analysis of particle transport in Barents-2.5 EPS is discussed in de Aguiar et al. (2023), but Figure 2 exemplifies the effect of flow field uncertainty on cluster of particles that have been advected using velocity fields from different ensemble members to showcase. We see that after 48 hours the particle clusters have taken a distinct shape based on the velocity field of the used ensemble member, and an estimated trajectory uncertainty can be obtained from the spread. The trajectory uncertainty is small when flow velocities are similar across the ensemble and increases when there is a large discrepancy between them.

5

2.3 The Finite Time Lyapunov Exponent

A particle will be advected in the presence of an underlying flow field. The trajectory may be obtained by integrating along the encountered flow field:

$$\boldsymbol{x}(t) = \boldsymbol{x}_0 + \int_{t_0}^{t} \boldsymbol{u}(\boldsymbol{x}(\tau))\,\mathrm{d}\tau. \tag{1}$$

Here, $\boldsymbol{x}(t)$ is the position of a particle at time t advected from its initial position $\boldsymbol{x}_0$ using the velocity field $\boldsymbol{u}$ along the evolving trajectory locations $\boldsymbol{x}(\tau)$. In this study, particle trajectories are calculated by OpenDrift (Dagestad et al., 2018), an open-source Python based software for Lagrangian particle modelling developed at the Norwegian Meteorological Institute.

The Lyapunov exponent describes the separation rate between two neighbouring particles in a chaotic system. This separation is assumed to grow exponentially over time so that the distance δ_t between the two particles at time t becomes

$$\delta_t \approx \delta_0 e^{\sigma t}, \tag{2}$$

where δ_0 is the initial separation and σ is the Lyapunov exponent, i.e. the separation rate (Rosenstein et al., 1993). FTLE finds the *maximum* separation rate between infinitesimal fluid parcels over a finite time-interval (Pierrehumbert and Yang, 1993).

FTLE's are calculated from flow fields provided by an OGCM following the method described by Haller (2001), Shadden et al. (2005) and Farazmand and Haller (2012). The 2D movement of fluid parcels from their initial positions $\boldsymbol{x}_0 = (x_0, y_0)$ at time t_0 to their final positions at time t is described by a flow map $\boldsymbol{F}_{t_0}^{t}(\boldsymbol{x}_0)$. As multiple fluid parcels are transported by the flow, the distance between neighbouring fluid parcels is likely to contract or expand over the time interval. At each point in space, the change in separation between fluid parcels can be described by the Jacobian of $\boldsymbol{F}_{t_0}^{t}(\boldsymbol{x}_0)$:

$$\boldsymbol{\nabla} \boldsymbol{F}_{t_0}^{t}(\boldsymbol{x}_0) = \begin{bmatrix} \frac{\partial x}{\partial x_0} & \frac{\partial x}{\partial y_0} \\ \frac{\partial y}{\partial x_0} & \frac{\partial y}{\partial y_0} \end{bmatrix}, \tag{3}$$

where (x, y) is the final position of a fluid parcel which was initially located at (x_0, y_0). These positions may be obtained from Eq. 1. The matrix entries in Eq. 3 are the partial derivatives of the final position relative to their initial position. Eq. 3 is used to define the Cauchy-Green strain tensor $\boldsymbol{C}_{t_0}^{t}(\boldsymbol{x}_0)$ (Truesdell and Noll, 2004), which describes the deformation in the system

$$\boldsymbol{C}_{t_0}^{t}(\boldsymbol{x}_0) = \left[\boldsymbol{\nabla} \boldsymbol{F}_{t_0}^{t}(\boldsymbol{x}_0)\right]^{*} \boldsymbol{\nabla} \boldsymbol{F}_{t_0}^{t}(\boldsymbol{x}_0). \tag{4}$$

the FTLE is then defined using $C_{t_0}^{t}$:

$$\sigma_{t_0}^{t}(\boldsymbol{x}) = \frac{1}{|T|} \ln \sqrt{\lambda_{max}\left(\boldsymbol{C}_{t_0}^{t}\right)}, \tag{5}$$

where T is the time interval over which the FTLE is computed and $\lambda_{max}\left(\boldsymbol{C}_{t_0}^{t}\right)$ is the largest eigenvalue of $\boldsymbol{C}_{t_0}^{t}(\boldsymbol{x}_0)$ corresponding to the dominant stretching direction (eigenvector) in the system. If one uses FTLE as an LCS detection tool, a forward-in-time computation will correspond to repelling LCS, whereas a backward-in-time computation will correspond to attracting LCS (Haller, 2001; Shadden et al., 2005; Farazmand and Haller, 2012).

In this study we will investigate FTLE computed from backward-in time integrations. Furthermore, the study is motivated by typical uses of ocean forecasting models, which are decision support tools for search-and-rescue operations, oil-spill and ice-berg forecasts and similar trajectory analyses. These often operate at time-scales from a few hours up to a few days, and therefore, we will predominantly use $T = 24$ hours for the FTLE computations. But we also provide some discussion of the choice of T in Sec. 3.1

FTLE averages over ensemble members and over time periods will be calculated to characterize robustness and persistence, respectively. For each such analysis, we first compute the FTLE fields from a set of flow fields and thereafter calculate averages over those FTLE fields, which is similar to the D-FTLE mean method discussed in Guo et al. (2016). We define the ensemble and time averages as:

$$\overline{F}_m = \frac{1}{N} \sum \sigma_{t_0}^t (m) \tag{6}$$

$$\overline{F}_t = \frac{1}{N} \sum \sigma_{t_0}^t (\tau), \tag{7}$$

where $\sigma_{t_0}^t (m)$ and $\sigma_{t_0}^t (\tau)$ are the FTLE fields over the given time interval for ensemble member m or over a specific time-period τ, and where N is the total number of fields being averaged. So, for example, for time interval $T = 24$ hours, τ will indicate the specific daily FTLE field from a set of multiple daily fields.

Variations among ensemble members and over time are expected due to perturbed and time-evolving velocity fields. It is thus expected that averaging FTLE fields will smooth out non-robust and non-persistent features while highlighting robust and persistent features, ultimately indicating regions where high FTLE values are statistically likely to form over ensemble members or frequently form over time. Certain features or 'ridges' in the averaged FTLE fields may also be discerned, in which case these should be considered highly robust or persistent. These regions are strong potential candidates for robust or persistent material accumulation regions.

We note that a time-average or ensemble average description of FTLE could also be performed by first averaging the flow field, and then calculating the FTLE. This procedure has the caveat that the flow maps used in Eqns. 2 and 3 is not based on time-evolving flow fields, and hence do not identify realistic deformation and accumulation. Instead, we aim for a statistical description of flow features by analysing the mean and spatial structure of realistic FTLE fields.

3 Results

Below, we first have a quick look at how the choice of integration time impacts the FTLE field, assessing this in relation to applications relevant for operational oceanography. We then look at whether there is in fact any persistence or robustness in FTLE fields over the dynamically active LoVe region. Finally, we do a spectral analysis of the FTLE field in an attempt at pin-pointing the resolution needed for practical use in an operational forecasting system.

3.1 Integration time

Backwards-in-time FTLE fields, all starting from the same t_0 at 2021-12-31 but using different integration lengths T, are shown in Figure 1. The values are normalized as the FTLE values tend to decrease with increasing T. As noted by e.g. Wilde et al.
175 (2018) and Peng and Dabiri (2008), a longer integration time tends to result in sharper FTLE ridges. We note, however, that the overall structure of the FTLE field is not overly sensitive to the integration period within the integration length of 12 to 72 hours, although the features in the field are more detailed for the 72-hour period than for 12 hours. For even longer integration periods there is clear indication that distinct FTLE features in the energetic flow regions over the continental shelf and slope are smeared out. A plausible interpretation is that the ability of the FTLE field to describe flow field features depends on the
180 integration period that matches the time scale of the dynamics. This advective time, which scales as L/U (for velocity scale U and length scale L), then depends on environmental conditions. So capturing highly energetic small-scale features associated with the fronts over the continental shelf and slope require short integration times. In contrast, low-energy and large-scale features over the deep basin are slow enough to be well-represented by FTLE integrations that have been conducted over several days.
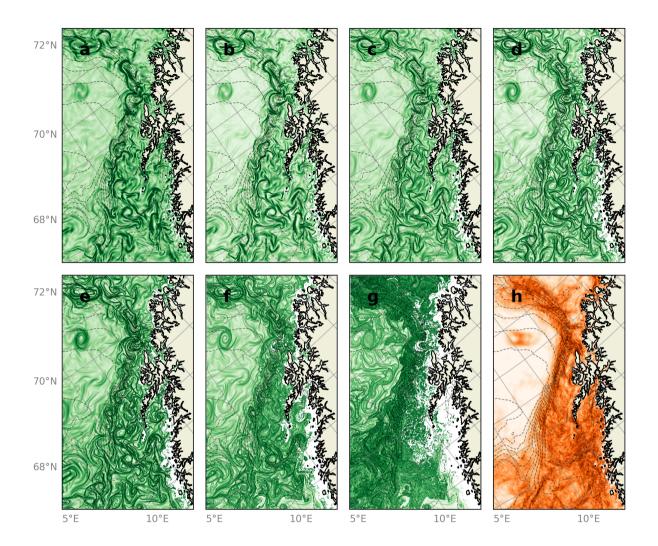
Figure 3. Normalized FTLE for computed for different values of T, all starting at 2021-12-31. a) 6 hours, b) 12 hours, c) 24 hours, d) 48 hours, e) 72 hours, f) 168 hours (7 days) and g) 672 hours (28 days). h) monthly average of FTLE fields computed with $T = 24$ hours. Bathymetry indicated with gray dashed lines.

A time-averaged FTLE field is also shown in Figure 3h. This is included to illustrate that the FTLE analysis based on long integration periods (e.g. over 168 and 672 hours) are distinctly different from the time-averaged FTLE field of several 24-hour integration periods. The time-averaged FTLE field should be interpreted as highlighting regions that are *typically* abundant with high FTLE values over the time period. The calculation reveals that in this particular region, structures forming high FTLE values are most often found over the continental slope. In contrast, the FTLE structures appearing over the deep basin when FTLEs are calculated over long integration periods wash out in the average description.

3.2 Persistence over time

Velocity magnitude fields and corresponding backwards FTLE fields from the first member of the Barents-2.5 EPS (henceforth called the reference member) are shown in Figure 3 for three example dates one week apart in January 2023, along with the monthly-averaged velocity and FTLE fields. As expected, the continental slope current is shown to be persistent over the time period. But the intensity and meandering of the current change from week to week, and this time variability projects onto the FTLE fields as few features there stay the same between time steps. And yet, there is clearly a concentration of high-magnitude FTLE features over the steep continental slope during this time period—as effectively summarized by the time-averaged FTLE field, $\overline{F}_t$. The interpretation is that strong FTLE features are expected to be frequent along the continental slope, at least over this sample time period, even though the FTLE average over time does not yield detailed information about how these look like as individual features.
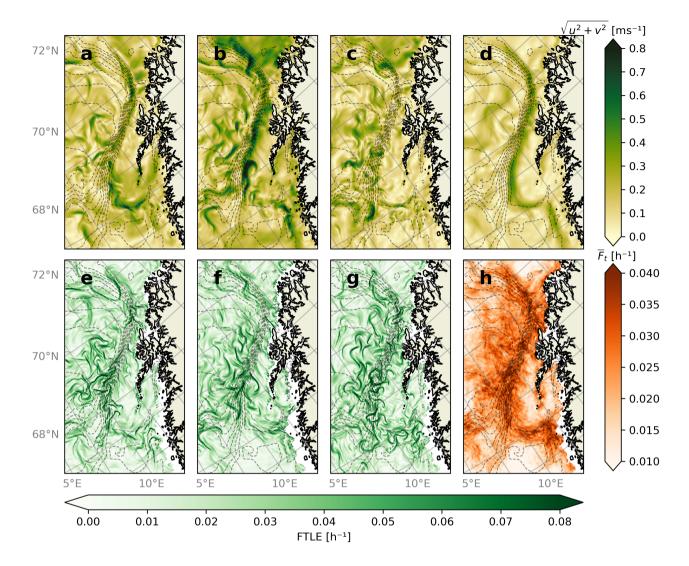
Figure 4. Instantaneous velocity fields (top row) from the reference member of Barents-2.5 EPS at a) 2023-01-02, b) 2023-01-08 and c) 2023-01-15 at 00:00. d) averaged velocity field for January 2023. Backwards FTLE fields (bottom row) computed with $T = 24$ hours over e) 2023-01-02 f) 2023-01-08 and c) 2023-01-15. h) monthly average of daily FTLE fields for January 2023. Gray dashed lines indicate bathymetry.

To highlight the permanent impact of the continental slope, seasonally-averaged velocity fields are shown in Figure 4 along with seasonal FTLE averages, $\overline{F}_t$, computed from daily FTLE fields from the summer and winter seasons. The slope current is placed similarly in both seasons, although it is stronger during winter, likely due to a geostrophic adjustment to the sea surface tilt, as discussed in Sec. 2.1. On the other hand, $\overline{F}_t$ changes drastically between the two seasons. We see that strong values in the FTLE field along the continental slope occur much more frequently during winter. Large values can be seen for both seasons near the coastline, which are suspected to be produced by strong horizontal velocity shear near the coastal regions.
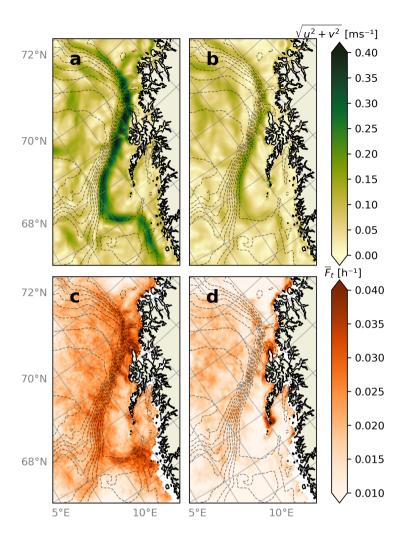
11

Figure 5. Seasonal FTLE averages for a) winter and b) summer. Months included in the winter season are December 2022, January 2023, and February 2023. Months included in summer season are June 2023, July 2023, and August 2023. Dashed gray lines indicate bathymetry.

Near the coast, a region of high $\overline{F}_t$ around Moskstraumen strait (at the southern tip of the LoVe archipelago; see Fig. 1), especially during summer, is directly connected to the formation of strong jets at the strait exit. The direction of the current through the strait is dependent on the tidal phase (Børve et al., 2021). After closer investigation using $T = 2$ hours for the FTLE time interval, high values in the FTLE field tend to form only on one side of Moskstraumen at any particular time, depending on the current direction and thus the tidal phase. Therefore, a predictable tidal-dependent periodic variability of FTLEs may exist here. FTLE has previously been shown to be highly sensitive to the tidal phase (Zhong et al., 2022). However, the models spatial resolution may be too low to fully resolve the currents in this region, and a closer investigation into the dynamics at play here will need to be left for a future high-resolution model study.

3.3 Robustness over ensemble realizations

We turn next to the concept of robustness of FTLE fields, that is the extent to which FTLE fields computed using flow fields from different EPS realizations are similar. As an example, velocity fields and FTLE fields of three randomly selected members are shown in Figure 6, along with the ensemble-averaged velocity and FTLE field. We see that the individual ensemble members all contain a strong current along the continental slope, which has also been shown to be a time-persistent current. However, and as expected from a highly nonlinear and chaotic flow field, the position and strength of individual eddies and current meanders vary considerably between members. This is certainly the case for small-scale structures along the slope current. But some larger-scale mesoscale structures over the deep ocean, e.g. a vortex in the south-western corner of the domain, are actually predicted by all three ensemble members. Such large-scale features thus survive the smoothing inherent in the ensemble-averaged velocity field, whereas most individual small-scale structures are washed out. Plainly speaking, the EPS gives a low confidence that any of these small-scale structures actually exist in the real ocean at their specific location at this particular time.
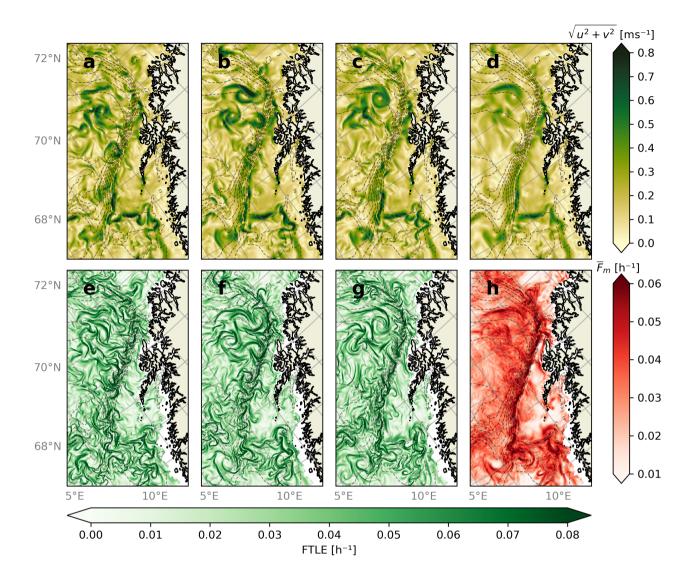
Figure 6. a, b and c) Velocity fields from three different Barents-2.5 EPS ensemble members at the LoVe region at 2023-02-02 00:00 and d) ensemble averaged velocity field over all EPS members. e, f and g) backwards FTLE fields computed over 2023-02-01 for the members shown in a, b and c. h) The ensemble averaged FTLE field.

The flow variability within the ensemble again projects directly onto the FTLE values, and, as expected, there is generally little one-to-one agreement between the three ensemble members displayed here. But we see that all the members of the ensemble predict high FTLE values along the continental slope, as well as in the eddy-dominated deep basin region at $70.5°$ latitude. But the exact positions and strength of FTLE maxima vary considerably and even more so than the velocity field itself. Again, we must interpret this as indication that the FTLE field from one single model integration may not reflect conditions in the real ocean at any specific time.

Thus, instead of inspecting the FTLE fields of each member individually, a study of the ensemble-averaged FTLE field, $\overline{F}_m$, allows us to detect robust flow features; high values will be present in $\overline{F}_m$ where multiple (but not necessarily all) individual members predict high FTLE activity. In the situation studied here, $\overline{F}_m$ shows a long and continuous feature tangent to the continental slope. However, in individual members the features formed by high FTLE values are seen to be disjointed, thinner and often not tangent to the continental slope. The eddy-dominated region at $70.5°$ latitude also contains high averaged FTLE values, but these are smoother than over the continental slope, thus presumably reflecting typical occurrences of strong FTLE features but also a lower impact of bottom bathymetry. An FTLE average may thus yield both distinguishable features in the domain, which can be considered as robust features, as well as large smooth fields of higher FTLE values, which indicate that strong features are likely to be found here but are more variable across the ensemble.

3.4 Properties of ensemble and time averaged FTLE fields

We wish to investigate how the energy distribution of FTLEs over different spatial scales change when averaged over the ensemble or time. One method for conducting the spectral analysis on 2D fields is the discrete cosine transform (DCT) proposed by Denis et al. (2002).

We select three 200km×200km non-overlapping sections of the domain away from landmasses. Following Denis et al. (2002), the DCT produces an N_i by N_j field $F(m, n)$ of spectral coefficients, where m and n are adimensional wavenumbers. For a square domain where $N_i = N_j = N$, the wavelength is given by

$$\lambda = \frac{2N\Delta}{k}, \tag{8}$$

where Δ is the grid spacing and $k = \sqrt{m^2 + n^2}$ is a normalized radial wavenumber. To study how the spectral variance of FTLE evolves with time and ensemble averaging, we first compute the average FTLE field over an increasing number of days and members. The results are shown in Figure 7 along with the spatial variance.
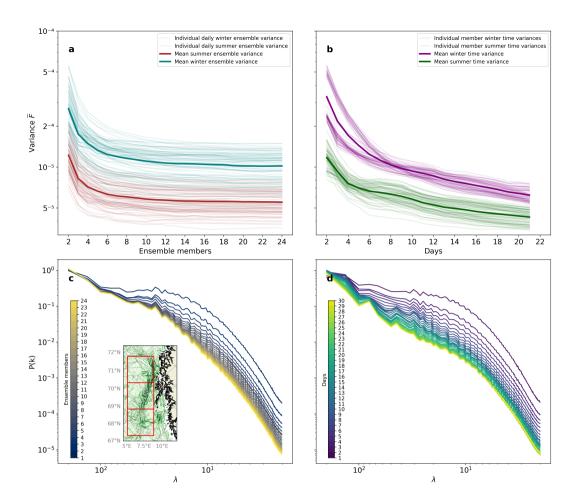
Figure 7. Spatial and spectral variance of FTLEs and averaged FTLEs. a) Spatial variance over the ensemble average. Thin blue and red graphs indicate individual days during the winter and summer seasons, and the thicker blue and red graphs are the average of the thin graphs. b) Spatial variance over the time average. Thin purple and green graphs indicate the evolution of variance during the winter and summer months as up to 21 days are considered in the time average for each member. c) Spectral distribution of spatial FTLE variance in ensemble averages as an increasing number of members are considered in the average, averaged over all days in January 2023. The red squares in the randomly selected FTLE field in c) indicate the regions selected the spectral variace computation. d) Spectral distribution of spatial FTLE variance for time averages as an increasing number of days are considered in the average, starting from 2023-01-01, averaged over all members. Colorbars in c) and d) indicate how many members or days the FTLE fields are averaged over.

The spatial variance has been computed by averaging FTLE fields from the three 200km×200km sections over an increasing number of members or days, then computing the variance over the resulting averaged FTLE field. Spatial variance ensures that
255 the degree of smoothing increases as more members or time steps are considered in the FTLE averages. The results suggest that the smoothing rate of FTLE fields is independent of season. The value of the variance is lower during summer as FTLE values are generally smaller compared to winter (Fig. 5). The strong decay at the beginning of the $\overline{F}_m$ variance implies that

there is a sufficient spread in the ensemble. Note that $\overline{F}_m$ depends on which members are included in the average for few members, which might affect the results as there is a possibility that any randomly selected member might deviate largely from other members. $\overline{F}_m$ becomes less sensitive to a strongly deviating member as more members are included in the average. The spatial variance of $\overline{F}_m$ stabilizes once ∼10 members are considered, implying the existence of distinct non-chaotic and highly predictable flow features in the ensemble. Meanwhile, the spatial variance of $\overline{F}_t$ continues diminishing, signifying that FTLE fields are more robust over many members than persistent over long time periods.

The spectral variance shows how energy is distributed over wavelengths. Energy diminishes as more members and time steps are included in the averages as a result of smoothing of the fields at all wavelengths, coherent with the smoothing factor in the spatial variance. Energy dissipates similarly for smaller wavelengths, and significantly faster for $\overline{F}_t$ than $\overline{F}_m$ for large to mid wavelengths. Small-scale flows and thus also small-scale FTLE features are generally chaotic and short-lived, and these are therefore uncertain between members and evolve rapidly over time. FTLE features are expected to smooth slower at large scales as flows are less chaotic here. Large-scale structures are more or less certain in the ensemble, whereas they are seen to evolve and drift over time at all scales (albeit slower at the largest wavelengths).

The decay of variance as more FTLE fields are included in an average (Fig. 7a vs. Fig 7b) indicates that FTLE features are more robust than persistent. The strong decline at the beginning of the spatial variance is due to small scale FTLE features experiencing a strong and quick smoothing due to averaging, and slows down afterwards as mostly large scale FTLE features are left. Robustness is particularly prominent at the larger spatial scales 7c, where little decay is noticed as more than 2-5 ensemble members are included in the average for large wavelengths. The spatial variance of $\overline{F}_m$ stabilizes as the large scale features that are left in the system are highly robust, whereas $\overline{F}_t$ continues being smoothed at all scales due the formation, drift, deformation and dissipation of FTLE features happening at all scales.

4 Summary and discussion

Features in ocean surface circulation, as described by FTLE analysis, have been investigated in terms of their *persistence* in time and *robustness* across EPS ensemble members. Statistics of FTLE, in this study mainly limited to the mean, were computed to assess their variability. Both smaller-scale details and large-scale features of the FTLE fields are variable over time and across ensemble members. Time and ensemble averages have therefore been computed as an attempt to identify robust and persistent FTLE features, respectively, while averaging out transient and uncertain features. Below we summarize and discuss some of the key findings.

4.1 FTLE as an indicator of LCS and transport barriers

LCSs describe attracting and repelling properties of fluid flows, as well as define transport barriers (Haller and Yuan, 2000; Farazmand and Haller, 2012; Haller, 2015). FTLE ridges have been discussed as possibly indicating the presence of LCSs, with clear limitations however. For instance, horizontal velocity shear may produce large FTLE values but will not yield material convergence towards or divergence away from the FTLE feature. Thus, such FTLE features are not indicative of LCSs (Haller,

2002; Branicki and Wiggins, 2010; Haller and Sapsis, 2011; Karrasch and Haller, 2013). Other limitations exist, but a strength of the FTLE approach is that it allows for simple statistical analysis of flow field features that in some instances point to the existence of LCSs.

At the very least, the systematic patterns in the FTLE fields over the continental slope off LoVe do suggest that the methods picks up important dynamical features. The current system in the study region is strongly impacted by a steep continental slope, which sets up a strong ambient potential vorticity (PV) gradient. As a result, a meandering current—guided by the bathymetry—will cause a recurring FTLE pattern, with implications for both robustness and persistence. Dong et al. (2021) also identified persistent FSLE in the LoVe region. Although FSLE generally does not coincide with FTLE (Karrasch and Haller, 2013), we find agreement in our results with Dong et al. (2021), who further showed that FSLE features hinder cross-slope transport. In other words, the FTLE and FSLE fields both seem to have detected a dynamical transport barrier (if not perfectly impenetrable) we know should exist from the ambient PV field.

A caveat in analysing FTLE fields in terms of their average is that details in shape and direction of individual FTLE ridges are lost. A ridge detection, that is the identification of what under ideal conditions will be LCS manifolds, could provide information on strain directionality, which may also be persistent under e.g. topographical current steering. Instead of averaging, one could follow a similar approach as Dong et al. (2021), where the authors defined a set of criterion for the existence of a particuler FSLE ridge and investigated the frequency with which the criterion was fulfilled. Another approach could be to select a particular FTLE ridge and study how it evolves over time. Its lifetime, propagation distance, growth/dissipation-rate and structural evolution could then be studied. Possibly, a relation between that FTLE ridge size, strength, and lifetime could be established.

As mentioned above, there are other, improved, proxies for LCSs. Duran et al. (2018) proposes a method for computing the climatology of LCSs using a so-called quasi-steady LCS method, yielding information about LCS persistence over a selected time period. This method is tested in the Brazilian current by Gouveia et al. (2020), where the authors state that large-scale flow features give rise to persistent quasi-steady LCSs. Quasi-steady LCS allows for more direct extraction of transport barriers than FTLE ridges, and may therefore be better suited for investigating the long-term climatology of particle transport of e.g. nutrients. Seeing that the method described by Duran et al. (2018) handles time averages, we argue for the potential of finding robust LCS transport barriers by combining ensemble methods with quasi-steady LCS, and propose this as a topic for future study. Similarly to FTLEs, if quasi-steady LCSs prove to be robust, the method could be used in operational oceanography to provide forecasts about e.g. possible search-and-rescue regions.

4.2 Temporal variability of FTLE

The analyses above confirm that the flow and associated FTLE field are seen to vary drastically over short time periods. Flow features that develop pronounced structures in the FTLE field will drift, deform and vanish over a range of time scales. Clearly, the lifetime of a particular FTLE feature is restricted by the lifetime of the flow structure it represents. Specifically, features formed by large-scale circulation as these typically imply longer time scales.

18

Permanent geomorphological features present a defining constraint on the ocean circulation and, in particular, large-scale bathymetry steers ocean currents at high latitudes (Gille et al., 2004). In the LoVe region, the persistent topographically-steered NCC and NwAC give rise to frequent high-valued FTLE features along the continental slope during winter (Fig. 5a). Individual FTLE features are hard to detect from the monthly-averaged FTLE field, but may be distinguished for shorter time averages where the smoothing effect due to averaging is smaller. The small-scale FTLE features, being more chaotic and short lived, are smoothed at the highest rate, whereas the large-scale FTLE anomalies remain visible for longer averaging times. Large-scale structures are expected to be more persistent.

Thus, time averaging of FTLE fields provides information about where FTLE features frequently form. However, we note that strong values in the FTLE average may sometimes result from infrequent but very strong FTLE values. Analysis of time-averaged FTLE is therefore useful for identifying regions of material accumulation and entrapment. For instance, we expect that the semi-permanent anti-cyclonic Lofoten Vortex (Fig. 1) in the middle of the Lofoten Basin (Raj et al., 2015; Isachsen, 2015) will form persistent and re-occurring FTLE features (Fig. 8). Furthermore, the canyons in the LoVe region host a multitude of aquatic organisms, e.g. cold water coral reefs, which is possible because of the nutrient accumulation here (Sundby et al., 2013; Bøe et al., 2016). We argue that these canyons will contribute to formation of persistent FTLE features, providing a control mechanism for particle transport towards specific locations.

4.3 Seasonal variability

Ocean currents in the LoVe region show seasonal variability in response to atmospheric forcing and the seasonally-varying hydrography. The autumn and winter months are characterized by westerly winds with transient low pressure systems passing through the region, and the water pile-up against the coast accelerates the currents. Spring and summer, in contrast, are dominated by moderate easterly winds (Furnes and Sundby, 1981) and weaker currents. In spring and summer, the seasonal stratification also responds to freshwater runoff and solar radiation (Christensen et al., 2018).

The associated seasonal ocean circulation patterns are reflected in the FTLE fields (Fig. 5. Most pronounced is a clear difference in the intensity of the FTLE field over the continental slope. A well-mixed water column during winter results in more barotropic flow, hence the bathymetry controls winter circulation and high FTLE values develop in the lateral shear region along topography-following slope currents. In contrast, seasonal stratification due to surface heating during summer leads to partial decoupling of the ocean surface layer from deeper currents, thus bathymetry has a weaker impact on surface flow structures during summer. Note that pronounced FTLE features may occur along the continental slope in summer, but these are less typical or weak, therefore tend to be washed out in both time and ensemble averages.

The coastline is expected to have a similar impact on FTLE formation throughout the year, as it directly affects surface currents, although near-shore FTLEs are suspected of mainly being produced by horizontal velocity shear. However, around Moskstraumen (Figs. 1 and 5) we identified higher FTLE variability in summer that is tied to tidal pumping through the narrow sound. Surface-intensified flow as a consequence of distinct summer stratification may amplify surface currents in this particular location (Sperrevik et al., 2017).

Finally, higher FTLE values during winter can be expected to be related to more energetic flows at scales of 1-100km. Circulation at this scale is intensified by baroclinic instabilities formed around geostrophic eddies, and are much stronger during winter than in summer (Callies et al., 2015).

4.4 Uncertainty of FTLEs in realistic flow fields

360 Ocean current uncertainty stems from non-linear equations of motion: small errors in initial or boundary conditions, as well as tunable parameter values, can cause large errors in numerical integrations (Lorenz, 1963). Error propagation may thus have impacts in trajectory simulations (e.g. Zimmerman, 1986; de Aguiar et al., 2023). By this argument, uncertainties in FTLE fields derived from uncertain currents are expected. Allshouse et al. (2017) discussed uncertainty from the impact of wind drag on surface FTLEs. In addition, we discuss the uncertainty due the flow field itself. A regional scale ocean EPS, Barents-2.5, is 365 here used to describes uncertainties of ocean currents in the analysis and throughout the forecast range (Idžanović et al., 2023). By calculating FTLE fields for each ensemble member, we propagate the ocean model uncertainty into the FTLE analysis presented here. The various members exhibit differences in the FTLE fields, e.g. in terms of feature location, intensity and shape. Generally, FTLE features that exist in only one or few members are statistically unlikely to exist (compare Fig. 6), emphasizing the need of an EPS when employing FTLE in operational oceanography.

370 Ensemble averaging is here suggested as a method to detect robust FTLE features, i.e. features that appear in a majority of members and can therefore be considered likely to exist, despite uncertainties in the underlying flow. Similarly to the time average, the ensemble average smooths out distinct features in the FTLE field, resulting in an average FTLE field $\overline{F}_m$ that highlights only the most predictable features. Some FTLE features can still be distinguished in $\overline{F}_m$, even after considering all 24 ensemble members of the Barents-2.5 EPS (Fig. 7). In particular, high FTLE areas located along the continental slope tend 375 to be more robust. As discussed above, the steep bathymetry plays an important role in causing the robustness, because even though the surface currents themselves are uncertain, the bathymetry constrains surface currents equally across the ensemble.

The spectral analysis (Fig. 7) confirmed our expectations that large-scale FTLE features are more robust, as variability does not decay at large wavelengths when increasing the number of ensemble members in the averaging beyond 2–4 members. Small-scale features, however, are effectively removed by the ensemble average because they are more chaotic and exhibiting 380 lower predictability. The conclusion is that FTLE features associated with larger-scale flows are more robust than small scale FTLEs.

Sensitivity of the FTLE method has previously been investigated using satellite altimetry products by Harrison and Glatz-maier (2012), where the authors conclude that FTLEs are fairly insensitive to noise included in the velocity fields and that FTLEs are robust for large-scale eddies and strong jets. Gouveia et al. (2020) argues that persistent large-scale features in 385 particular give rise to quasi-steady LCS, such as the feature reported by Dong et al. (2021) which is also analyzed in our study. In addition to time-persistent features, we investigate FTLE detection from transient flow features. Importantly, the Barents-2.5 EPS model used in this study can represent smaller and more transient structures than the aforementioned satellite products. From this we found that high FTLE areas are more uncertain at smaller scales, but robust where the flow is constrained by coastal or bathymetric steering.

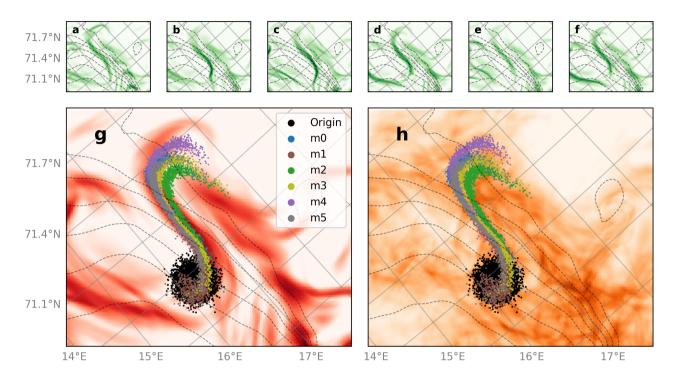**4.5   Implications for operational forecasting**

Figure 8. FTLE averages and particle clusters advected using velocity fields from a small number of different Barents-2.5 EPS ensemble members. Panels a-f show the 24-hour FTLE fields from each member used to advect the particles, while panels g and h show the ensemble averaged FTLE field and the monthly averaged FTLE field from one member, respectively. Black dots in panels g and h mark the initial position of the particles on 2023-01-01, and their final positions after four days.

Operational use of FTLE analysis in forecasting, e.g. for search-and-rescue, oil-spill operations or path-planning (e.g. Beegle-Krause et al., 2011; Ramos et al., 2018; Serra et al., 2020), should be viewed in context of the uncertainty in ocean current predictions. And although FTLE fields are variable across an ensemble, we have seen that some features of the FTLE field are more robust than others. An ensemble of FTLEs must thus be assessed to separate robust from non-robust features. The

395   detection of a robust FTLE feature would thus present an opportunity to accurately identify search regions and dispatch environmental clean-up resources.

Fig 8 illustrates the power of ensemble averaging. It shows a situation where there happens to be high agreement between particle cluster trajectories over four days from a few different, randomly selected, ensemble realizations. The ensemble-averaged FTLE field over all 24 ensemble members is also shown and appears to be highly robust: FTLE features remain

400   clearly articulated in the average. More importantly, particle clusters from all ensemble members are seen to be attracted towards the nearby high values of $\overline{F}_m$. Thus, in such a case, the ensemble-averaged FTLE field provides a clear added value to trajectory forecasting in a real-time setting.

In contrast to this, the 30-day FTLE average from a single ensemble member, shown in Fig. 8, does not shed much light on the short-term particle trajectories in this particular situation. This should not come as a surprise, as the FTLE features will have

405 evolved substantially over the month. It is likely that certain FTLE features may be distinguished in shorter-term averages, taken over e.g. 3–4 days, could be utilized for short-term forecasting. However, in that case it may be more appropriate to compute the FTLE field with $T = 3$ days instead, then obtaining the ensemble-averaged FTLE field over the time interval.

5   Conclusions

FTLEs are clearly imperfect representations of LCSs. And yet, FTLE analysis provides a practical diagnostic tool for analyzing

410 how ocean flow morphology associated with deformation impacts particle transport. In this numerical model study we have examined how the uncertainty of ocean model forecasts, illustrated in an ocean EPS, propagates into FTLE fields. It was shown that by employing ensemble averaging of ensemble FTLE fields, robust features of the FTLE field, that is features which the EPS system has gotten right in a statistical sense, may be separated from uncertain, non-robust, features. In particular, ensemble averaging typically retains flow structures at larger scales that are time-evolving but predictable at specific times.

415 The averaging will more typically wash out FTLE structures present in individual ensemble members, but it still has the potential to highlight regions over which FTLE features are statistically likely to emerge. Such features are often influenced by geomorphological constraints which, in our specific study region, was exemplified by a steep continental slope that imposes strong—and permanent—ambient PV gradients. We have also shown how such permanent environmental constraints can make FTLE fields persistent in time. Large seasonal variations in atmospheric forcing and hydrographic conditions can impact both

420 the robustness and persistence of FLTE structures, but the FTLE fields studied here were generally shown to be more robust than persistent. So the over-all lesson learned from the study is that FTLE analysis can indeed add value to operational forecasting, even in light of the highly nonlinear and chaotic nature of real ocean flows. The key requirement is the forecast is treated as a probabilistic one, most practically produced using ensemble techniques.

References

Adlandsvik, B. and Sundby, S.: Modelling the transport of cod larvae from the Lofoten area, ICES Marine Science Symposia, 198, 379–392, 1994.

435 Allshouse, M. R., Ivey, G. N., Lowe, R. J., Jones, N. L., Beegle-Krause, C. J., Xu, J., and Peacock, T.: Impact of windage on ocean surface Lagrangian coherent structures, Environmental Fluid Mechanics, 17, 473–483, https://doi.org/10.1007/s10652-016-9499-3, 2017.

Balasuriya, S.: Explicit invariant manifolds and specialised trajectories in a class of unsteady flows, Physics of Fluids, 24, 127 101, https://doi.org/10.1063/1.4769979, 2012.

Balasuriya, S.: Uncertainty in finite-time Lyapunov exponent computations, Journal of Computational Dynamics, 7, 313–337,
440 https://doi.org/10.3934/jcd.2020013, 2020.

Balasuriya, S., Kalampattel, R., and Ouellette, N. T.: Hyperbolic neighbourhoods as organizers of finite-time exponential stretching, Journal of Fluid Mechanics, 807, 509–545, https://doi.org/10.1017/jfm.2016.633, 2016.

Beegle-Krause, C. J., Peacock, T., and Allshouse, M.: Exploiting Lagrangian coherent structures (LCS) for the calculation of oil spill and search-and-rescue drift patterns in the ocean, https://www.osti.gov/etdeweb/biblio/21547684, 2011.

445 Branicki, M. and Wiggins, S.: Finite-time Lagrangian transport analysis: stable and unstable manifolds of hyperbolic trajectories and finite-time Lyapunov exponents, Nonlinear Processes in Geophysics, 17, 1–36, https://doi.org/10.5194/npg-17-1-2010, 2010.

Brunton, S. L. and Rowley, C. W.: Fast computation of finite-time Lyapunov exponent fields for unsteady flows, Chaos: An Interdisciplinary Journal of Nonlinear Science, 20, 017 503, https://doi.org/10.1063/1.3270044, 2010.

Bøe, R., Bellec, V. K., Dolan, M. F. J., Buhl-Mortensen, P., Rise, L., and Buhl-Mortensen, L.: Cold-water coral reefs in the Hola glacial
450 trough off Vesterålen, North Norway, Geological Society, London, Memoirs, 46, 309–310, https://doi.org/10.1144/M46.8, 2016.

Børve, E., Isachsen, P. E., and Nøst, O. A.: Rectified tidal transport in Lofoten–Vesterålen, northern Norway, Ocean Science, 17, 1753–1773, https://doi.org/10.5194/os-17-1753-2021, 2021.

Callies, J., Callies, J., Ferrari, R., Klymak, J. M., and Gula, J.: Seasonality in submesoscale turbulence, Nature communications, 6, 6862, https://doi.org/10.1038/ncomms7862, 2015.

455 Christensen, K. H., Sperrevik, A. K., and Broström, G.: On the Variability in the Onset of the Norwegian Coastal Current, Journal of Physical Oceanography, 48, 723 – 738, https://doi.org/10.1175/JPO-D-17-0117.1, 2018.

Dagestad, K.-F., Röhrs, J., Breivik, Ø., and Ådlandsvik, B.: OpenDrift v1.0: a generic framework for trajectory modelling, Geoscientific Model Development, 11, 1405–1420, https://doi.org/10.5194/gmd-11-1405-2018, 2018.

de Aguiar, V., Röhrs, J., Johansson, A. M., and Eltoft, T.: Assessing ocean ensemble drift predictions by comparison with observed oil slicks,
460 Frontiers in Marine Science, 10, https://doi.org/10.3389/fmars.2023.1122192, 2023.

Denis, B., Côté, J., and Laprise, R.: Spectral Decomposition of Two-Dimensional Atmospheric Fields on Limited-Area Domains Using the Discrete Cosine Transform (DCT), Monthly Weather Review, 130, 1812 – 1829, https://doi.org/10.1175/1520-0493(2002)130<1812:SDOTDA>2.0.CO;2, 2002.

Dong, H., Zhou, M., Hu, Z., Zhang, Z., Zhong, Y., Basedow, S. L., and Smith Jr., W. O.: Transport Barriers and the Retention
465 of Calanus finmarchicus on the Lofoten Shelf in Early Spring, Journal of Geophysical Research: Oceans, 126, e2021JC017 408, https://doi.org/10.1029/2021JC017408, 2021.

d'Ovidio, F., Fernández, V., Hernández-García, E., and López, C.: Mixing structures in the Mediterranean Sea from finite-size Lyapunov exponents, Geophysical Research Letters, 31, https://doi.org/10.1029/2004GL020328, 2004.

Duran, R., Beron-Vera, F., and Olascoaga, M.: Extracting quasi-steady Lagrangian transport patterns from the ocean circulation: An application to the Gulf of Mexico, Scientific reports, 8, 5218, https://doi.org/10.1038/s41598-018-23121-y, 2018.

Evensen, G.: Inverse methods and data assimilation in nonlinear ocean models, Physica D: Nonlinear Phenomena, 77, 108–129, https://doi.org/10.1016/0167-2789(94)90130-9, 1994.

Farazmand, M. and Haller, G.: Computing Lagrangian coherent structures from their variational theory, Chaos: An Interdisciplinary Journal of Nonlinear Science, 22, 013 128, https://doi.org/10.1063/1.3690153, 2012.

Furnes, G. and Sundby, S.: Upwelling and wind induced circulation in Vestfjorden, The Norwegian Coastal Current, Proceedings from the Norwegian Coastal Current Symposium, 1, 152–177, 1981.

Gascard, J.-C., Raisbeck, G., Sequeira, S., Yiou, F., and Mork, K. A.: The Norwegian Atlantic Current in the Lofoten basin inferred from hydrological and tracer data (129I) and its interaction with the Norwegian Coastal Current, Geophysical Research Letters, 31, https://doi.org/10.1029/2003GL018303, 2004.

Ghosh, A., Suara, K., McCue, S. W., Yu, Y., Soomere, T., and Brown, R. J.: Persistency of debris accumulation in tidal estuaries using Lagrangian coherent structures, Science of The Total Environment, 781, 146 808, https://doi.org/10.1016/j.scitotenv.2021.146808, 2021.

Gille, S., Metzger, J., and Tokmakian, R.: Seafloor Topography and Ocean Circulation, Oceanography, 17, 47–54, https://doi.org/10.5670/oceanog.2004.66, 2004.

Giudici, A., Suara, K. A., Soomere, T., and Brown, R.: Tracking areas with increased likelihood of surface particle aggregation in the Gulf of Finland: A first look at persistent Lagrangian Coherent Structures (LCS), Journal of Marine Systems, 217, 103 514, https://doi.org/https://doi.org/10.1016/j.jmarsys.2021.103514, 2021.

Gouveia, M. B., Duran, R., Lorenzzetti, J. A., Assireu, A. T., Toste, R., Assad, L. P. d. F., and Gherardi, D. F. M.: Persistent meanders and eddies lead to a quasi-steady Lagrangian transport pattern in a weak western boundary current, Scientific reports, https://doi.org/10.48550/arXiv.2008.07620, 2020.

Guo, H., He, W., Peterka, T., Shen, H.-W., Collis, S. M., and Helmus, J. J.: Finite-Time Lyapunov Exponents and Lagrangian Coherent Structures in Uncertain Unsteady Flows, IEEE Transactions on Visualization and Computer Graphics, 22, 1672–1682, https://doi.org/10.1109/TVCG.2016.2534560, 2016.

Hadjighasem, A., Farazmand, M., Blazevski, D., Froyland, G., and Haller, G.: A critical comparison of Lagrangian methods for coherent structure detection, Chaos: An Interdisciplinary Journal of Nonlinear Science, 27, 053 104, https://doi.org/10.1063/1.4982720, 2017.

Haller, G.: Distinguished material surfaces and coherent structures in three-dimensional fluid flows, Physica D: Nonlinear Phenomena, 149, 248–277, https://doi.org/10.1016/S0167-2789(00)00199-8, 2001.

Haller, G.: Lagrangian coherent structures from approximate velocity data, Physics of Fluids, 14, 1851–1861, https://doi.org/10.1063/1.1477449, 2002.

Haller, G.: A variational theory of hyperbolic Lagrangian Coherent Structures, Physica D: Nonlinear Phenomena, 240, 574–598, https://doi.org/10.1016/j.physd.2010.11.010, 2011.

Haller, G.: Lagrangian Coherent Structures, Annual Review of Fluid Mechanics, 47, 137–162, https://doi.org/10.1146/annurev-fluid-010313-141322, 2015.

Haller, G. and Sapsis, T.: Lagrangian coherent structures and the smallest finite-time Lyapunov exponent, Chaos: An Interdisciplinary Journal of Nonlinear Science, 21, 023 115, https://doi.org/10.1063/1.3579597, publisher: American Institute of Physics, 2011.

Haller, G. and Yuan, G.: Lagrangian coherent structures and mixing in two-dimensional turbulence, Physica D: Nonlinear Phenomena, 147, 352–370, https://doi.org/10.1016/S0167-2789(00)00142-1, 2000.

Harrison, C. S. and Glatzmaier, G. A.: Lagrangian coherent structures in the California Current System – sensitivities and limitations, Geophysical & Astrophysical Fluid Dynamics, 106, 22–44, https://doi.org/10.1080/03091929.2010.532793, 2012.

Hussain, A. K. M. F.: Coherent structures—reality and myth, The Physics of Fluids, 26, 2816–2850, https://doi.org/10.1063/1.864048, 1983.

510 Idžanović, M., Rikardsen, E. S. U., and Röhrs, J.: Forecast uncertainty and ensemble spread in surface currents from a regional ocean model, Frontiers in Marine Science, 10, https://doi.org/10.3389/fmars.2023.1177337, 2023.

Isachsen, P. E.: Baroclinic instability and the mesoscale eddy field around the Lofoten Basin, Journal of Geophysical Research: Oceans, 120, 2884–2903, https://doi.org/10.1002/2014JC010448, 2015.

Karrasch, D. and Haller, G.: Do Finite-Size Lyapunov Exponents detect coherent structures?, Chaos: An Interdisciplinary Journal of Nonlin-
515 ear Science, 23, 043 126, https://doi.org/10.1063/1.4837075, 2013.

Koszalka, I., LaCasce, J. H., and Mauritzen, C.: In pursuit of anomalies—Analyzing the poleward transport of Atlantic Water with surface drifters, Deep Sea Research Part II: Topical Studies in Oceanography, 85, 96–108, https://doi.org/10.1016/j.dsr2.2012.07.035, 2013.

Krishna, K., Brunton, S. L., and Song, Z.: Finite Time Lyapunov Exponent Analysis of Model Predictive Control and Reinforcement Learn-
ing, https://arxiv.org/abs/2304.03326, 2023.

520 Lebreton, L. C. M., Greer, S. D., and Borrero, J. C.: Numerical modelling of floating debris in the world's oceans, Marine Pollution Bulletin, 64, 653–661, https://doi.org/10.1016/j.marpolbul.2011.10.027, 2012.

Lee, Y.-K., Shih, C., Tabeling, P., and Ho, C.-M.: Experimental study and nonlinear dynamic analysis of time-periodic micro chaotic mixers, Journal of Fluid Mechanics, 575, 425–448, https://doi.org/10.1017/S0022112006004289, 2007.

Lekien, F., Coulliette, C., Mariano, A. J., Ryan, E. H., Shay, L. K., Haller, G., and Marsden, J.: Pollution release tied to invariant manifolds:
525 A case study for the coast of Florida, Physica D: Nonlinear Phenomena, 210, 1–20, https://doi.org/10.1016/j.physd.2005.06.023, 2005.

Lorenz, E. N.: Deterministic Nonperiodic Flow, Journal of Atmospheric Sciences, 20, 130 – 141, https://doi.org/10.1175/1520-0469(1963)020<0130:DNF>2.0.CO;2, 1963.

Lou, Q., Li, Z., Zhang, X., Xiang, X., and Cao, Z.: Lagrangian analysis of material transport around the headland in the Yellow River Estuary, Frontiers in Marine Science, 9, https://doi.org/10.3389/fmars.2022.999367, 2022.

530 Matuszak, M.: mateuszmatu/LCS: FTLE computation software release for article, https://doi.org/10.5281/zenodo.10797134, 2024.

Mitchelson-Jacob, G. and Sundby, S.: Eddies of Vestfjorden, Norway, Continental Shelf Research, 21, 1901–1918, https://doi.org/10.1016/S0278-4343(01)00030-9, 2001.

Müller, M., Homleid, M., Ivarsson, K.-I., Køltzow, M. A. O., Lindskog, M., Midtbø, K. H., Andrae, U., Aspelien, T., Berggren, L., Bjørge, D., Dahlgren, P., Kristiansen, J., Randriamampianina, R., Ridal, M., and Vignes, O.: AROME-MetCoOp: A Nordic Convective-Scale
535 Operational Weather Prediction Model, Weather and Forecasting, 32, 609–627, https://doi.org/10.1175/WAF-D-16-0099.1, 2017.

Norwegian Meteorological Institute: Barents-2.5 ocean and ice forecast model archive, [data set] last acess 2024-04-29, https://thredds.met.no/thredds/fou-hi/barents_eps.html.

Olascoaga, M. J. and Haller, G.: Forecasting sudden changes in environmental pollution patterns, Proceedings of the National Academy of Sciences, 109, 4738–4743, https://doi.org/10.1073/pnas.1118574109, 2012.

540 Olascoaga, M. J., Rypina, I. I., Brown, M. G., Beron-Vera, F. J., Koçak, H., Brand, L. E., Halliwell, G. R., and Shay, L. K.: Persistent transport barrier on the West Florida Shelf, Geophysical Research Letters, 33, https://doi.org/https://doi.org/10.1029/2006GL027800, 2006.

Peacock, T. and Haller, G.: Lagrangian coherent structures: The hidden skeleton of fluid flows, Physics Today, 66, 41–47, https://doi.org/10.1063/PT.3.1886, 2013.

Peng, J. and Dabiri, J. O.: The 'upstream wake' of swimming and flying animals and its correlation with propulsive efficiency, Journal of Experimental Biology, 211, 2669–2677, https://doi.org/10.1242/jeb.015883, 2008.

Pierrehumbert, R. T. and Yang, H.: Global Chaotic Mixing on Isentropic Surfaces, Journal of the Atmospheric Sciences, 50, 2462–2480, https://doi.org/10.1175/1520-0469(1993)050<2462:GCMOIS>2.0.CO;2, 1993.

Raj, R. P., Chafik, L., Nilsen, J. E. O., Eldevik, T., and Halo, I.: The Lofoten Vortex of the Nordic Seas, Deep Sea Research Part I: Oceanographic Research Papers, 96, 1–14, https://doi.org/10.1016/j.dsr.2014.10.011, 2015.

Ramos, A. G., García-Garrido, V. J., Mancho, A. M., Wiggins, S., Coca, J., Glenn, S., Schofield, O., Kohut, J., Aragon, D., Kerfoot, J., Haskins, T., Miles, T., Haldeman, C., Strandskov, N., Allsup, B., Jones, C., and Shapiro, J.: Lagrangian coherent structure assisted path planning for transoceanic autonomous underwater vehicle missions, Scientific Reports, 8, 4575, https://doi.org/10.1038/s41598-018-23028-8, 2018.

Rosenstein, M. T., Collins, J. J., and De Luca, C. J.: A practical method for calculating largest Lyapunov exponents from small data sets, Physica D: Nonlinear Phenomena, 65, 117–134, https://doi.org/10.1016/0167-2789(93)90009-P, 1993.

Rossby, T., Ozhigin, V., Ivshin, V., and Bacon, S.: An isopycnal view of the Nordic Seas hydrography with focus on properties of the Lofoten Basin, Deep Sea Research Part I: Oceanographic Research Papers, 56, 1955–1971, https://doi.org/10.1016/j.dsr.2009.07.005, 2009.

Röhrs, J., Christensen, K. H., Vikebø, F., Sundby, S., Saetra, O., and Broström, G.: Wave-induced transport and vertical mixing of pelagic eggs and larvae, Limnology and Oceanography, 59, 1213–1227, https://doi.org/10.4319/lo.2014.59.4.1213, 2014.

Röhrs, J., Gusdal, Y., Rikardsen, E., Duran Moro, M., Brændshøi, J., Kristensen, N. M., Fritzner, S., Wang, K., Sperrevik, A. K., Idžanović, M., Lavergne, T., Debernard, J., and Christensen, K. H.: Barents-2.5km v2.0: An operational data-assimilative coupled ocean and sea ice ensemble prediction model for the Barents Sea and Svalbard, Geoscientific Model Development Discussions, pp. 1–31, https://doi.org/10.5194/gmd-2023-20, 2023.

Samelson, R.: Lagrangian Motion, Coherent Structures, and Lines of Persistent Material Strain, Annual Review of Marine Science, 5, 137–163, https://doi.org/10.1146/annurev-marine-120710-100819, 2013.

Serra, M., Sathe, P., Rypina, I., Kirincich, A., Ross, S. D., Lermusiaux, P., Allen, A., Peacock, T., and Haller, G.: Search and rescue at sea aided by hidden flow structures, Nature Communications, 11, 2525, https://doi.org/10.1038/s41467-020-16281-x, 2020.

Shadden, S. C., Lekien, F., and Marsden, J. E.: Definition and properties of Lagrangian coherent structures from finite-time Lyapunov exponents in two-dimensional aperiodic flows, Physica D: Nonlinear Phenomena, 212, 271–304, https://doi.org/10.1016/j.physd.2005.10.007, 2005.

Shchepetkin, A. F. and McWilliams, J. C.: The regional oceanic modeling system (ROMS): a split-explicit, free-surface, topography-following-coordinate oceanic model, Ocean Modelling, 9, 347–404, https://doi.org/10.1016/j.ocemod.2004.08.002, 2005.

Sperrevik, A. K., Röhrs, J., and Christensen, K. H.: Impact of data assimilation on Eulerian versus Lagrangian estimates of upper ocean transport, Journal of Geophysical Research: Oceans, 122, 5445–5457, https://doi.org/10.1002/2016JC012640, 2017.

Sundby, S.: Influence of bottom topography on the circulation at the continental shelf off northern Norway, Fiskeridirektoratets Skrifter Serie Havundersokelser, 17, 501–519, 1984.

Sundby, S. and Bratland, P.: Spatial distribution and production of eggs from Northeast-arctic cod at the coast of Northern Norway 1983–1985, Fisken og havet, 1, 1987.

Sundby, S., Fossum, P., Sandvik, A. D., Vikebø, F., Aglen, A., Buhl-Mortensen, L., Folkvord, A., Bakkeplass, K., Buhl-Mortensen, P., Johannessen, M., Jørgensen, M. S., Kristiansen, T., Landra, C. S., Myksvoll, M. S., and Nash, R. D. M.: KunnskapsInnhenting Barentshavet–Lofoten–Vesterålen (KILO), 188 s., https://imr.brage.unit.no/imr-xmlui/handle/11250/113923, publisher: Havforskningsinstituttet, last access: 17 April 2024, 2013.

Tang, W., Chan, P. W., and Haller, G.: Accurate extraction of Lagrangian coherent structures over finite domains with application to flight data analysis over Hong Kong International Airport, Chaos: An Interdisciplinary Journal of Nonlinear Science, 20, 017 502, https://doi.org/10.1063/1.3276061, 2010.

585 Thoppil, P. G., Frolov, S., Rowley, C. D., Reynolds, C. A., Jacobs, G. A., Joseph Metzger, E., Hogan, P. J., Barton, N., Wallcraft, A. J., Smedstad, O. M., and Shriver, J. F.: Ensemble forecasting greatly expands the prediction horizon for ocean mesoscale variability, Communications Earth and Environment, 2, 89, https://doi.org/10.1038/s43247-021-00151-5, 2021.

Trodahl, M. and Isachsen, P. E.: Topographic Influence on Baroclinic Instability and the Mesoscale Eddy Field in the Northern North Atlantic Ocean and the Nordic Seas, Journal of Physical Oceanography, 48, 2593–2607, https://doi.org/10.1175/JPO-D-17-0220.1, 2018.

590 Truesdell, C. and Noll, W.: The Non-Linear Field Theories of Mechanics, in: The Non-Linear Field Theories of Mechanics, edited by Truesdell, C., Noll, W., and Antman, S. S., pp. 57–73, Springer, Berlin, Heidelberg, https://doi.org/10.1007/978-3-662-10388-3_1, 2004.

van Sebille, E., Griffies, S. M., Abernathey, R., Adams, T. P., Berloff, P., Biastoch, A., Blanke, B., Chassignet, E. P., Cheng, Y., Cotter, C. J., Deleersnijder, E., Döös, K., Drake, H. F., Drijfhout, S., Gary, S. F., Heemink, A. W., Kjellsson, J., Koszalka, I. M., Lange, M., Lique, C., MacGilchrist, G. A., Marsh, R., Mayorga Adame, C. G., McAdam, R., Nencioli, F., Paris, C. B., Piggott, M. D., Polton, J. A., Rühs, S.,
595 Shah, S. H. A. M., Thomas, M. D., Wang, J., Wolfram, P. J., Zanna, L., and Zika, J. D.: Lagrangian ocean analysis: Fundamentals and practices, Ocean Modelling, 121, 49–75, https://doi.org/10.1016/j.ocemod.2017.11.008, 2018.

Wei, M., Jacobs, G., Rowley, C., Barron, C. N., Hogan, P., Spence, P., Smedstad, O. M., Martin, P., Muscarella, P., and Coelho, E.: The impact of initial spread calibration on the RELO ensemble and its application to Lagrangian dynamics, Nonlinear Processes in Geophysics, 20, 621–641, https://doi.org/10.5194/npg-20-621-2013, 2013.

600 Wei, M., Jacobs, G., Rowley, C., Barron, C. N., Hogan, P., Spence, P., Smedstad, O. M., Martin, P., Muscarella, P., and Coelho, E.: The performance of the US Navy's RELO ensemble, NCOM, HYCOM during the period of GLAD at-sea experiment in the Gulf of Mexico, Deep Sea Research Part II: Topical Studies in Oceanography, 129, 374–393, https://doi.org/10.1016/j.dsr2.2013.09.002, the Gulf of Mexico Ecosystem - before, during and after the Macondo Blowout, 2016.

Wilde, T., Rössl, C., and Theisel, H.: FTLE Ridge Lines for Long Integration Times, in: 2018 IEEE Scientific Visualization Conference
605 (SciVis), pp. 57–61, https://doi.org/10.1109/SciVis.2018.8823761, 2018.

Zhong, X., Wu, Y., Hannah, C., Li, S., and Niu, H.: Applying finite-time lyapunov exponent to study the tidal dispersion on oil spill trajectory in Burrard Inlet, Journal of Hazardous Materials, 437, 129 404, https://doi.org/10.1016/j.jhazmat.2022.129404, 2022.

Zimmerman, J.: The tidal whirlpool: A review of horizontal dispersion by tidal and residual currents, Netherlands Journal of Sea Research, 20, 133–154, https://doi.org/10.1016/0077-7579(86)90037-2, 1986.

610 Zimmermann, J., Motejat, M., Rössl, C., and Theisel, H.: FTLE for Flow Ensembles by Optimal Domain Displacement, arXiv e-prints, https://arxiv.org/abs/2401.04153, 2024.